Escape from planetary neighbourhoods

Waalkens, H.; Burbanks, A.; Wiggins, S.

Published in:
Monthly Notices of the Royal Astronomical Society

DOI:
10.1111/j.1365-2966.2005.09237.x

Publication date:
2005

Mon. Not. R. Astron. Soc. **361,** 763–775 (2005) doi:10.1111/j.1365-2966.2005.09237.x

Escape from planetary neighbourhoods

H. Waalkens,⋆ A. Burbanks⋆ and S. Wiggins⋆
School of Mathematics, University of Bristol, University Walk, Bristol BS8 1TW

Accepted 2005 May 23. Received 2005 May 5; in original form 2005 March 4

ABSTRACT

In this paper we use recently developed phase-space transport theory coupled with a so-called classical spectral theorem to develop a dynamically exact and computationally efficient procedure for studying escape from a planetary neighbourhood. The 'planetary neighbourhood' is a bounded region of phase space where entrance and escape are only possible by entering or exiting narrow 'bottlenecks' created by the influence of a saddle point. The method therefore immediately applies to, for example, the circular restricted three-body problem and Hill's lunar problem (which we use to illustrate the results), but it also applies to more complex, and higher-dimensional, systems possessing the relevant phase-space structure. It is shown how one can efficiently compute the mean passage time through the planetary neighbourhood, the phase-space flux in, and out, of the planetary neighbourhood, the phase-space volume of initial conditions corresponding to trajectories that escape from the planetary neighbourhood, and the fraction of initial conditions in the planetary neighbourhood corresponding to bound trajectories. These quantities are computed for Hill's problem. We study the dependence of the proportions of these quantities on energy and dimensionality (two-dimensional planar and three-dimensional spatial Hill's problem). The methods and quantities presented are of central interest for many celestial and stellar dynamical applications such as, for example, the capture and escape of moons near giant planets, the formation of binaries in the Kuiper belt and the escape of stars from star clusters orbiting about a galaxy.

Key words: methods: *N*-body simulations – celestial mechanics – planets and satellites: formation – planetary systems: formation.

1 INTRODUCTION

Escape from a 'planetary neighbourhood' is a fundamental problem in celestial mechanics. The crux of the problem lies in giving a precise definition of what is meant by 'the neighbourhood of a planet', and with this in hand one can then consider the dynamical issues associated with entrance to, and exit from, this neighbourhood. Now there are many papers on escape and capture in celestial mechanics settings (see, for example, Heppenheimer & Porco 1977; Petit & Hénon 1986; Murison 1989; Tanikawa, Kikuchi & Sato 1991; Belbruno & Marsden 1997; Cordeiro, Martins & Leonel 1999; Heggie 2001; Winter & Neto 2001; Yu & Tremaine 2001; Astakhov et al. 2003; Astakhov & Farrelly 2004; Makó & Szenkovits 2004), which would lead one to question what we will develop here that is really new. This can be answered by focusing on the quantities that we wish to compute. For example, consider the mean passage time for trajectories that enter and exit a planetary neighbourhood. Computing this quantity requires knowledge of a specific type of trajectory (or else the averaging leads to inaccuracies). Of course, brute-force Monte Carlo sampling can be used to approximate such results. However, there are still two points to be made here. One is that knowledge of a certain type of trajectory is still required, which can be obtained with a sufficient brute-force sampling. The second point, which follows from the very last remark, is that, for three dimensions, brute-force approaches such as Monte Carlo may be prohibitively time-consuming, and expensive. Another quantity that we wish to compute is the flux of trajectories into, or out of, the planetary neighbourhood. The flux is the volume of trajectories crossing a surface per unit time. This definition also implies consideration of a trajectory exhibiting a specified type of behaviour. However, there is slightly more: a surface that defines entrance, or exit, to the planetary neighbourhood. Such a surface must be carefully chosen because a bad choice might easily lead to trajectories that cross the surface and immediately turn back. Taking account of such trajectories in the calculation of the flux of entering or escaping trajectories will lead to an overestimation of this quantity.

These exact same issues have received a great deal of attention in the chemistry literature, where the 'transference of allegiance' from one planet to another is analogous to a chemical reaction. The relevant theory from chemistry goes by the name of transition state

⋆E-mail: H.Waalkens@bris.ac.uk (HW); A.Burbanks@bris.ac.uk (AB); S.Wiggins@bris.ac.uk (SW)

theory, and was first described by Eyring (1934) and Wigner (1937, 1938), and was applied in a two-dimensional celestial mechanics setting related to asteroid capture by Jaffé et al. (2002). The central problem with applying this theory is the construction of a 'surface of no return'. For two-dimensional systems this was solved by Pollak, Child & Pechukas (1980), Child & Pollak (1980), Pechukas & McLafferty (1973), Pechukas & Pollak (1978) and Pechukas (1976). In making the transition to three dimensions, and higher, fundamentally new problems arise, and these have been addressed in a series of papers (Wiggins 1990b, 1992, 1994; Wiggins et al. 2001; Uzer et al. 2001; Waalkens, Burbanks & Wiggins 2004), which form the theoretical framework for the results of this paper. In three dimensions the surface of no return must be constructed in phase space (it can be argued that such a surface cannot generally be constructed in configuration space), and an algorithm for its construction exists. With this surface in hand, one can then compute flux and the mean passage time, described above. Combining these two results with a result which, in the chemistry literature, is known as a classical spectral theorem (Pollak 1981) allows us to compute the volume of initial conditions corresponding to trajectories that escape from the planetary neighbourhood. This result, along with the volume of the planetary neighbourhood, allows us to compute the fraction of initial conditions in the planetary neighbourhood that lead to bound (i.e. non-escaping) trajectories.

Returning to the statements at the beginning of this introduction, while we have discussed a 'surface of no return' and quantities related to trajectories that cross it, we have not given a precise description of what we mean by a 'planetary neighbourhood' and how the surface controls access to this neighbourhood. This is an issue that is both problem- and energy-dependent, and requires an understanding of the global structure of the energy surface. Saddle points also play an important role (but the influence of the saddle must be coupled with knowledge of the global structure of the energy surface). In the circular restricted three-body problem (CRTBP) and Hill's lunar problem for energies 'near' L_1 and L_2 the zero velocity surfaces (ZVS) in configuration space contribute to a natural definition of planetary neighbourhood in a way that is easily transferred to the relevant structures in phase space. For simplicity of introduction of our phase-space transport approach to planetary escape and capture, we consider Hill's lunar problem in this paper. However, the application to the CRTBP, and other problems exhibiting the relevant phase-space structure, is straightforward. This paper is organized as follows.

In Section 2 we provide a general description of the phase-space structures governing transport in the three-dimensional Hill's problem. We then turn to the planar Hill's problem where in Section 3.1 we compute the structures governing transport in phase space and show their projections into configuration space. In the process we illustrate some of the misconceptions that can arise from attempting to deduce dynamical consequences from projections into configuration space. In Section 3.2 we show how one can compute the mean passage time, flux, volume of initial conditions corresponding to escaping trajectories, and the fraction of initial conditions corresponding to trajectories that remain trapped, in a way that avoids brute-force sampling of the planetary neighbourhood. We do this for three different energies. In the process we describe the origin of a fractal structure associated with these trajectories described earlier by Murison (1989) through the choice of an 'optimal' surface of section. The problem of the appropriate choice of a surface of section that will reveal dynamical phenomena of interest is well known, and we provide such a choice for studying capture and escape that is easily constructed for either two or three dimensions. We next turn our attention to the spatial problem and in Section 4.1 we compute the phase-space structures governing transport in phase space and show their projections into configuration space. It is here where we get a first glimpse of the fundamental differences in the capture and escape problem between two and three dimensions. In Section 4.2 we compute the mean passage time, flux, volume of initial conditions corresponding to escaping trajectories, and the fraction of initial conditions corresponding to trajectories that remain trapped for the same three energies that we considered for the 2d problem. Finally, in the conclusions, we compare the capture and escape problem for two and three dimensions and give a discussion of the computational effort required with our approach compared with brute-force Monte Carlo sampling.

2 HILL'S PROBLEM AND THE PHASE-SPACE STRUCTURE NEAR L_1 AND L_2

The CRTBP models the motion of a tiny particle under the gravitational influence of one (large) primary mass and one (smaller) secondary mass both in circular orbits about their common centre of mass (Murray & Dermott 1999). Hill's problem is a limit version of the CRTBP which describes the motion of the particle in a neighbourhood of the secondary mass. The dimensionless spatial Hill's equations can be derived from the Hamiltonian

$$H = \frac{1}{2}\left(p_x^2 + p_y^2 + p_z^2\right) + yp_x - xp_y - x^2 + \frac{1}{2}(y^2 + z^2) - \frac{3}{r} \tag{1}$$

where $r = (x^2 + y^2 + z^2)^{1/2}$. We will also consider the planar Hill's problem; the invariant two-degrees-of-freedom (2-DOF) subsystem which has $z = p_z = 0$. Among other things, we are interested in the differences between the 2-DOF and the 3-DOF systems.

Hill's equations are not invariant under time reversal, due to the Coriolis forces, which Hill's problem inherits from the rotating coordinate system in the CRTBP. However, Hill's equations are invariant under the transformation $\mathcal{S}$ that maps the phase space coordinates and time according to

$$\mathcal{S} : (x, y, z, p_x, p_y, p_z, t) \mapsto (-x, y, z, p_x, -p_y, -p_z, -t). \tag{2}$$

It is well known that the spatial Hill's equations have two equilibria at $(x, y, z, p_x, p_y, p_z) = (-1, 0, 0, 0, -1, 0)$ and $(x, y, z, p_x, p_y, p_z) = (1, 0, 0, 0, 1, 0)$; the Lagrange points L_1 and L_2 which are related by the symmetry (2). The energy of L_1 and L_2 is $E_0 = -4.5$. The matrices associated with linearizing Hamilton's equations about each equilibrium have a pair of real eigenvalues of equal magnitude and opposite sign $\pm\sqrt{2\sqrt{7}+1}$, and two pairs of pure imaginary complex conjugate eigenvalues $\pm$i 2 and $\pm\mathrm{i}\sqrt{2\sqrt{7}-1}$. This means that L_1 and L_2 are equilibria of saddle–centre–centre type. The planar system has eigenvalues $\pm\sqrt{2\sqrt{7}+1}$ and $\pm\mathrm{i}\sqrt{2\sqrt{7}-1}$, i.e. the equilibria are of saddle–centre type.

A detailed theory for phase-space transport near saddle–centre –. . .–centre equilibrium points (which we refer to as 'saddles' for short in the following) has been developed in recent years (Wiggins 1990b, 1992, 1994; Uzer et al. 2001; Wiggins et al. 2001; Waalkens et al. 2004). For energies slightly above that of the saddle, on each $(2n-1)$-dimensional energy surface with n being the number of degrees of freedom, there exists an invariant $(2n-3)$-dimensional sphere S^{2n-3} of saddle stability type. This $(2n-3)$-sphere is significant for two reasons, as follows.

(i) It is the 'equator' of a $(2n-2)$-dimensional sphere, the so-called dividing surface. The equator separates the dividing surface into two hemispheres which have the structure of open $(2n-2)$-dimensional balls. Except for the equator (which is an invariant manifold), the dividing surface is locally a 'surface of no return' in the sense that trajectories which have crossed the dividing surface must leave a certain neighbourhood of the dividing surface before they can possibly cross the dividing surface again. For energies 'sufficiently close' to the energy of the saddle, the dividing surface satisfies the bottleneck property. This means that the energy surface has locally the geometrical structure of $S^{2n-2} \times I$, i.e. $(2n-2)$-sphere $\times$ interval, and the dividing surface divides the energy surface into two disjoint components. Moreover, the only way a trajectory can pass from one component of the energy surface to the other in the forward direction is through one hemisphere and the only way to pass in the backward direction is through the other hemisphere. The hemispheres thus are the gateways to the exit and entrance channels for the energy surface components. The forward and backward flux through the hemispheres are of equal magnitude and opposite sign so that the total flux through the dividing surface is zero. However, for our particular choice of dividing surface, the directional flux is minimal in a sense made precise by Waalkens & Wiggins (2004).

(ii) The $(2n-3)$-sphere is a normally hyperbolic invariant manifold (NHIM; Wiggins 1994). Normal hyperbolicity means that the expansion and contraction rates of the dynamics on the $(2n-3)$-sphere are dominated by those transverse to it. Just like a 'saddle point' the NHIM therefore has stable and unstable manifolds. In this case, the stable and unstable manifolds are $(2n-2)$-dimensional, having the structure of spherical cylinders, $S^{2n-3} \times I$, where I is an interval. Hence, they are of one less dimension than the energy surface and act as 'separatrices'; they 'enclose' a volume of the energy surface. Their key dynamical significance is that the only way that trajectories can pass through the dividing surface is if they are inside a certain region of the energy surface enclosed by the stable and unstable spherical cylinders.

For $n = 2$ DOF the NHIM is a one-dimensional sphere S^1; it is the unstable periodic orbit, the so-called Lyapunov periodic orbit, associated with the saddle. The Lyapunov periodic orbits associated with L_1 and L_2 in the planar Hill's problem correspond to orbit families c and a, respectively, in the nomenclature of Hénon (1969) and Strömgren. There exist various elaborate methods for computing the periodic orbit as well as its stable and unstable manifolds (see, for example, Simó & Stuchi 2000; Henrard & Navarro 2001, and references therein, for an application to the planar Hill's problem). In the 1970s and in the context of chemical reactions, Pechukas & McLafferty (1973), Pechukas & Pollak (1978) and Pollak et al. (1980) showed how, for 2-DOF systems of type 'kinetic-plus-potential', the periodic orbit can be used to construct a dividing surface, the so-called periodic orbit dividing surface (PODS), which has the bottleneck property mentioned above. Although the PODS theory can be extended to certain types of 2-DOF systems which are not of the simple type kinetic-plus-potential (Jaffé, Farrelly & Uzer 1999, 2000), we here follow a different approach based on a Poincaré–Birkhoff normalization procedure. This approach has the advantage that, unlike the PODS construction, it has no principle limitations concerning the number of DOF or type of Hamiltonian function (Uzer et al. 2001).

For $n = 3$ DOF the NHIM is a 3-sphere S^3, its stable and unstable manifolds are spherical cylinders $S^3 \times \mathbb{R}$ and the dividing surface is a four-dimensional sphere S^4. As we will explain in more detail in Sections 3.1 and 4.1, the Poincaré–Birkhoff normalization procedure gives explicit formulae for the NHIM, its stable and unstable manifolds, and the dividing surface in terms of 'normal form coordinates' (Uzer et al. 2001). The phase-space structures are then mapped into the original coordinates by the inverse of the normal form (NF) transformation.

Because the NFs about L_1 and L_2 are related by the symmetry (2) it is sufficient to compute explicitly only the NF about L_1. As a result of the two complex eigenvalues associated with the equilibria being rationally independent, the NF for the spatial Hill's problem, to any desired finite order of computation, is completely integrable with integrals given by $\mathcal{I} = p_1 q_1$, $J_k = (1/2)(q_k^2 + p_k^2)$, $k = 2, 3$. Here the (q_k, p_k), $k = 1, 2, 3$, are the canonically conjugate pairs of coordinates for the normal form. The corresponding Hamiltonian can be written solely as a function of the integrals, $H_{\rm NF} = H_{\rm NF}(\mathcal{I}, J_2, J_3)$, and Hamilton's equations decouple into the product of independent linear systems

$$(\dot{q}_1, \dot{p}_1) = \frac{\partial H_{\rm NF}}{\partial \mathcal{I}}(q_1, -p_1),$$
$$(\dot{q}_k, \dot{p}_k) = \frac{\partial H_{\rm NF}}{\partial J_k}(p_k, -q_k), \qquad k = 2, 3. \tag{3}$$

In terms of the NF coordinates it can be shown that the planar Hill's problem again appears as an invariant subsystem of the spatial problem. This is a consequence of the fact that for the linearized equations of motions the (z, p_z) DOF decouple from the planar system. We order the NF coordinates so that the planar system has $q_3 = p_3 = 0$. Accordingly, the NF Hamiltonian for the planar system is $H_{\rm NF;planar}(\mathcal{I}, J_2) = H_{\rm NF}(\mathcal{I}, J_2, 0)$.

It is important to understand how the normal form is used to compute phase-space structures because, in general, we do not expect the normal form expansion to converge (see Birkhoff 1927; Siegel 1952, 1954; Rüssmann 1964; Gustavson 1966; Arnol'd, Kozlov & Neishtadt 1988, for an overview). The goal is to obtain a neighbourhood of the saddle in phase space that is as large as possible, in which the approximation resulting from the truncation of the NF (to some finite order) yields the 'desired accuracy'. What we mean by 'desired accuracy', and how we determine it, will be explained shortly. This 'neighbourhood of validity' of the NF in phase space has to be large enough to contain the dividing surface (and hence the NHIM, which is itself contained in the dividing surface) for the energy of interest. The larger the neighbourhood of validity, the higher one can go in energy above the energy of the saddle in order to compute the dividing surface, the NHIM, and the local parts of its stable and unstable manifolds. For a given neighbourhood of an equilibrium point, we take the NF computation to successively higher orders until either no improvement in accuracy is seen with increasing order, or the desired accuracy is reached.

Using the transformations back and forth between the NF coordinates and the original phase-space coordinates, the accuracy of the NF is determined by a battery of checks, which include the conservation of the original Hamiltonian on the computed dividing surface (which contains the NHIM), invariance of the computed NHIM under the original Hamiltonian flow, and conservation of the integrals resulting from the NF along trajectories computed by integrating the original equations of motion as they pass through the neighbourhood under consideration.

We note that existence, and persistence, of the NHIM are independent of any NF computation. At high enough energy, however, the NHIM might undergo a bifurcation (little is known about bifurcations of normally hyperbolic 3-spheres). For smaller energies, it is also true that the motion on the NHIM might become more complicated than that described by the NF. For example, by

arguments from KAM theory one expects the tori that foliate the NHIM to break up. The existence of the Lyapunov periodic orbit (planar problem) or, more generally, the NHIM (spatial problem) is only a necessary but not a sufficient condition for the construction of our dividing surfaces. We take a pragmatic approach and suggest, therefore, that when the level of accuracy is insufficient for a particular application, then one varies the degree to which the NF computation is taken to detect whether sufficient accuracy can be reached for the chosen energy.

We perform the NF computation, using the computer-algebra system MATHEMATICA, up to degree 18 (i.e. the NF Hamiltonian may be written as a sum of homogeneous polynomials of degree up to 18 in the normal form coordinates). As a result, the NF Hamiltonian is a sum over 219 multivariate monomials in $(\mathcal{I}, J_2, J_3)$. Each component of the mapping between NF coordinates and the original phase-space coordinates involves sums over about 50 000 multivariate monomials. For this NF and for the energies considered below, the integrals $(\mathcal{I}, J_2, J_3)$ are conserved to 12 digits and more along trajectories as they traverse through the neighbourhood of validity that we define for this NF.

For some of the considerations below it is important to note that, up to the energies we consider, $H_{\rm NF}(\mathcal{I}, J_2, J_3)$ is a monotonically increasing function with respect to each of its components, i.e. $\partial H_{\rm NF}/\partial\mathcal{I}, \partial H_{\rm NF}/\partial J_2, \partial H_{\rm NF}/\partial J_3 > 0$.

The high quality of the local NF approximations of the local parts of the stable and unstable manifolds of the NHIM allows us to extend or 'globalize' these manifolds far away from the neighbourhood of validity of the NF by integrating the original equations of motion. At this stage we mention that we perform a regularization of the collision singularity in the original equations of motion by the Kustaanheimo–Stiefel transformation (Stiefel & Scheifele 1971).

3 PLANAR HILL'S PROBLEM

For the planar system, the motion in configuration space is confined by the level sets of the effective potential energy

$$V \equiv H - \frac{1}{2}\left[(p_x + y)^2 + (p_y - x)^2\right] = -\frac{3}{2}x^2 - \frac{3}{r}. \qquad (4)$$

These so-called zero velocity curves are shown in Fig. 1. For energies less than the energy E_0 of the Lagrange points, the zero velocity curves delimit a neighbourhood of the planet from which trajectories cannot escape. For energies slightly above E_0 the neighbourhood opens near L_1 and L_2, i.e. trajectories passing near L_1 or L_2 can escape or enter the planetary neighbourhood. As we will discuss in detail in the following section, the dividing surfaces near L_1 and L_2 are the bottlenecks to escape and capture. For an energy slightly above E_0 the dividing surfaces divide the energy surfaces into three disjoint components: the unbound region, which projects to the left of L_1 in Fig. 1; the unbound region, which projects the right of L_2 in Fig. 1; and a bound region by which we define the planetary neighbourhood for an energy $E > E_0$.

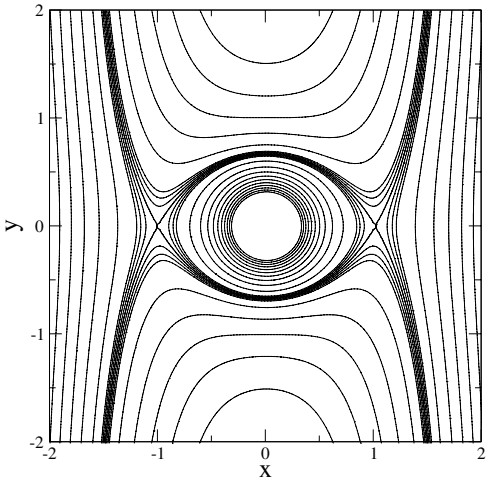

Figure 1. Planar Hill's problem. Zero velocity curves for energies $E = E_0 + n\Delta E$, with $\Delta E = 0.05$ for $n = -3, \ldots, 3$ and $\Delta E = 0.5$ for $n = -10, \ldots, 5$. L_1 and L_2 have configuration space coordinates $(x, y) = (-1, 0)$ and $(x, y) = (1, 0)$, respectively.

3.1 Phase-space conduits for transport across the bottlenecks near L_1 and L_2 in the planar system

As mentioned in Section 2, the local phase-space structure and dynamics near L_1 and L_2 can be unfolded using the NF. For a fixed energy E slightly above E_0, Fig. 2 shows the various manifolds mentioned in Section 2 for the saddle L_1 as projections to the saddle plane (q_1, p_1) and the centre plane (q_2, p_2). The projection of the energy surface is marked light blue. In the saddle plane (q_1, p_1) the projection of the energy surface is bounded by the two branches of the hyperbola $p_1 q_1 = \mathcal{I}$ (outer blue lines in Figs 2a and c) with $\mathcal{I}$ being implicitly defined by $H_{\rm NF;planar}(\mathcal{I}, 0) = E$; it is unbounded in the centre plane (q_2, p_2).

The dividing surface 2-sphere, which we denote by $S^2_{\rm ds}(L_1)$, has $p_1 = q_1$. In the saddle plane, $S^2_{\rm ds}(L_1)$ projects to the segment $q_1 = p_1$ (solid red/green line segment in Fig. 2c) with endpoints $q_1 = p_1 = \pm\sqrt{\mathcal{I}}$ with $\mathcal{I}$ being implicitly defined by $H_{\rm NF;planar}(\mathcal{I}, 0) = E$. The

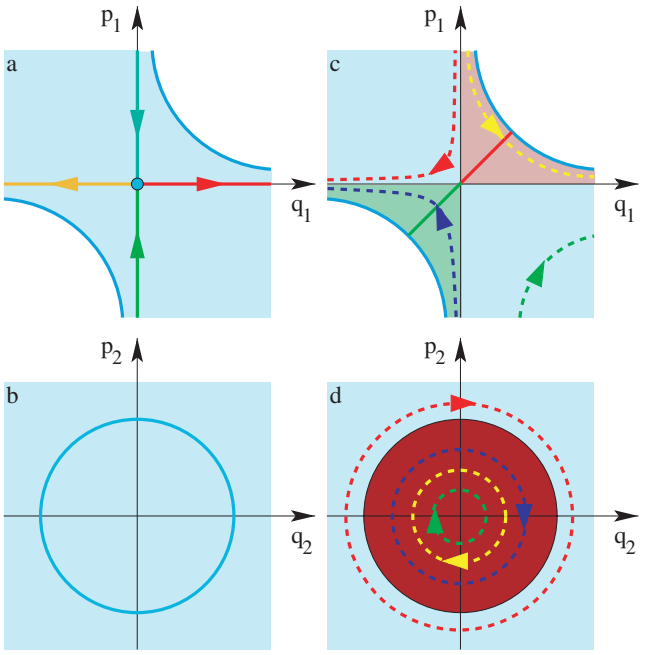

Figure 2. Planar Hill's problem. Schematic plot of the manifolds near L_1 as projections to the NF coordinate planes. (a) and (b) show the projections of the NHIM and its stable and unstable manifolds to the saddle and centre plane, respectively. (c) and (d) show the projections of the dividing surface, the capture and escape cylinders and the capture and escape volumes they enclose (see text). (c) and (d) also show representative orbits: the dashed yellow line marks a captured orbit, the blue dashed line marks an escaping orbit, and the red and green dashed lines correspond to orbits that are not captured and do not escape, respectively.

projection of $S^2_{\rm ds}(\mathrm{L}_1)$ to the centre plane is a disc (marked dark red in Fig. 2d) with boundary $(p_2^2 + q_2^2)/2 = J_2$ with J_2 being implicitly defined by $H_{\rm NF;planar}(0, J_2) = E$. The dividing surface locally divides the energy surface into two components $p_1 - q_1 > 0$ and $p_1 - q_1 < 0$. In physical space these components correspond to (pieces of) the unbound region of negative x and the planetary neighbourhood, respectively.

The NHIM near L_1 is the Lyapunov periodic orbit of L_1 and we denote it by $S^1_{\rm NHIM}(\mathrm{L}_1)$. It has $q_1 = p_1 = 0$ and hence projects to the origin in the saddle plane (the blue point at the origin in Fig. 2a). In the centre plane, it projects to the circle (marked blue in Fig. 2b) that bounds the projection of $S^2_{\rm ds}(\mathrm{L}_1)$. The periodic orbit $S^1_{\rm NHIM}(\mathrm{L}_1)$ separates $S^2_{\rm ds}(\mathrm{L}_1)$ into two hemispheres: a capture hemisphere $B^2_{\rm c}(\mathrm{L}_1)$ and an escape hemisphere $B^2_{\rm e}(\mathrm{L}_1)$. The hemispheres have the structure of two-dimensional open discs, or equivalently, two-dimensional open balls. In the saddle plane, they project to the parts $q_1 = p_1 > 0$ and $q_1 = p_1 < 0$, respectively, of the segment $p_1 = q_1 = 0$ that corresponds to $S^2_{\rm ds}(\mathrm{L}_1)$ (see the red and green line segments in Fig. 2c). All trajectories which enter the planetary neighbourhood from the unbound region of negative x have to cross the capture hemisphere $B^2_{\rm c}(\mathrm{L}_1)$; all trajectories which escape from the planetary neighbourhood into the unbound region of negative x have to cross the escape hemisphere $B^2_{\rm e}(\mathrm{L}_1)$.

The NHIM has stable and unstable manifolds $W^{\rm s}(\mathrm{L}_1)$ and $W^{\rm u}(\mathrm{L}_1)$ with the structure of cylinders $S^1 \times \mathbb{R}$. They have $q_1 = 0$ and $p_1 = 0$, respectively. Their projections to the saddle plane coincide with the coordinate axes; their projections to the centre plane coincide with the projection of the NHIM (see Figs 2a and b). The stable and unstable manifolds each have two branches which we call escape and capture branches, respectively. We denote the stable capture branch $q_1 = 0$, $p_1 > 0$ by $W^{\rm s}_{\rm c}(\mathrm{L}_1)$ and the unstable capture branch which has $q_1 > 0$, $p_1 = 0$ by $W^{\rm u}_{\rm c}(\mathrm{L}_1)$. The stable and unstable escape branches are denoted by $W^{\rm s}_{\rm e}(\mathrm{L}_1)$ ($q_1 = 0$, $p_1 < 0$) and $W^{\rm u}_{\rm e}(\mathrm{L}_1)$ ($q_1 < 0$, $p_1 = 0$), respectively. We call the union of the capture branches $W^{\rm s}_{\rm c}(\mathrm{L}_1) \cup W^{\rm u}_{\rm c}(\mathrm{L}_1)$ the capture cylinder and the union of the escape branches $W^{\rm s}_{\rm e}(\mathrm{L}_1) \cup W^{\rm u}_{\rm e}(\mathrm{L}_1)$ the escape cylinder associated with L_1. The significance of the capture and escape cylinders is that they enclose the volumes which contain all captured and all escaping trajectories, respectively. These volumes project to the region enclosed by the hyperbola branches of the projection of the energy surface in the second and third quadrants of the saddle plane, respectively (marked light red and light green in Fig. 2c); their projections to the centre plane coincide with the projection of the dividing surface.

Fig. 3 shows the manifolds computed from the NF as projections to the (x, y) configuration space of the original coordinates. The colour scheme is the same as in Fig. 2. It is worth mentioning that the boundaries of the configuration space projection of the volumes enclosed by the escape and capture cylinders do not coincide with the boundaries of the configuration space projection of the escape and capture cylinders themselves. In fact, the configuration space projection of the enclosed volumes is larger, as can be seen from comparing Figs 3(d), (e) and (f). This leads, at first sight, to the confusing effect that a trajectory, which, in phase space, is contained in the volume enclosed by the escape or capture cylinder, may not project to the region in configuration space covered by the projection of that cylinder. Note that a similar effect already occurred for the projection to the saddle plane in Fig. 2(a) in which the cylinders project to lines, i.e. they do not bound the projection of the volume they enclose in phase space from both sides (see Fig. 2c). The effect for the configuration space projection can be viewed as a strong indication that the often taken purely configuration space oriented point of view may not be conclusive or may even be wrong.

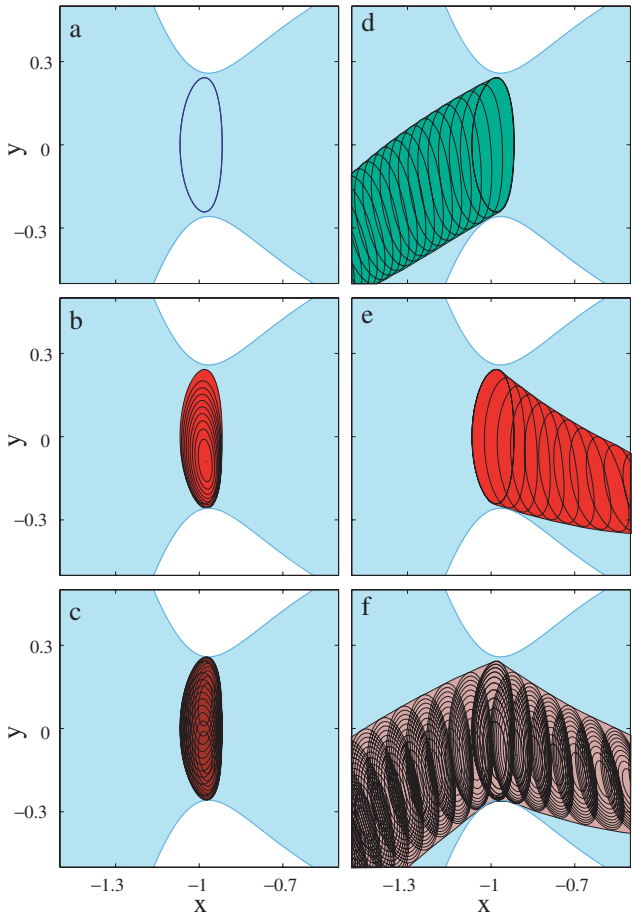

Figure 3. Planar Hill's problem. Manifolds near L_1 as projections to the (x, y) configuration space: (a) the NHIM (the Lyapunov periodic orbit); (b) the capture dividing surface hemisphere $B^2_{\rm c}(\mathrm{L}_1)$; (c) the complete dividing surface $S^2_{\rm ds}(\mathrm{L}_1)$; (d) the stable and (e) the unstable capture branches $W^{\rm s}_{\rm c}(\mathrm{L}_1)$ and $W^{\rm u}_{\rm c}(\mathrm{L}_1)$; (f) the projection of the energy surface volume of captured orbits enclosed by the capture cylinder $W^{\rm s}_{\rm c}(\mathrm{L}_1) \cup W^{\rm u}_{\rm c}(\mathrm{L}_1)$. The colour scheme is the same as in Fig. 2. The energy is $E = -4.4$.

The manifolds associated with L_2 can be obtained from the symmetry transformation $\mathcal{S}$ defined in equation (2) which relates the manifolds associated with L_1 and L_2 according to

$$\begin{aligned} S^1_{\rm NHIM}(\mathrm{L}_1) &\leftrightarrow S^1_{\rm NHIM}(\mathrm{L}_2), \quad S^2_{\rm ds}(\mathrm{L}_1) \leftrightarrow S^2_{\rm ds}(\mathrm{L}_2), \\ B^2_{\rm e}(\mathrm{L}_1) &\leftrightarrow B^2_{\rm c}(\mathrm{L}_2), \quad B^2_{\rm c}(\mathrm{L}_1) \leftrightarrow B^2_{\rm e}(\mathrm{L}_2), \\ W^{\rm s}_{\rm e}(\mathrm{L}_1) &\leftrightarrow W^{\rm u}_{\rm c}(\mathrm{L}_2), \quad W^{\rm u}_{\rm e}(\mathrm{L}_1) \leftrightarrow W^{\rm s}_{\rm c}(\mathrm{L}_2), \\ W^{\rm s}_{\rm c}(\mathrm{L}_1) &\leftrightarrow W^{\rm u}_{\rm e}(\mathrm{L}_2), \quad W^{\rm u}_{\rm c}(\mathrm{L}_1) \leftrightarrow W^{\rm s}_{\rm e}(\mathrm{L}_2). \end{aligned} \tag{5}$$

Here we have used '$\leftrightarrow$' to indicate that, due to $\mathcal{S}^{-1} = \mathcal{S}$, the manifolds are mapped to each other by $\mathcal{S}$ in either direction.

3.2 Escape from the planetary neighbourhood in the planar system

For fixed values of the energy E above E_0 we now study the escape from the planetary neighbourhood defined above. More precisely, we will determine the portion of initial conditions in the planetary neighbourhood, which when integrated with Hill's equations lead to trajectories that eventually escape from the planetary

neighbourhood. For comparison we start with a computationally expensive brute-force approach in which we sample phase-space points in the planetary neighbourhood and integrate them to find out whether they escape or not. We then compare the results obtained this way with our approach which utilizes the phase-space structures explained above. As we will show, the latter approach is not only much more elegant but also computationally cheaper than the brute-force sampling of the first method.

For the first approach we initialize phase-space points uniformly with respect to the measure $\delta(E - H)\,\mathrm{d}x\,\mathrm{d}y\,\mathrm{d}p_x\,\mathrm{d}p_y$ in the planetary neighbourhood for the energy E under consideration and integrate them in time until they either reach one of the dividing surfaces $S^2_{\mathrm{ds}}(\mathrm{L}_1)$ and $S^2_{\mathrm{ds}}(\mathrm{L}_2)$ or reach a large fixed cut-off time which is chosen such that escape after this time is very unlikely. For the planar case, we find that the cut-off time $t_{\mathrm{cut-off}} = 200$ is suitable for this purpose. In order to sample the initial conditions uniformly with respect to the energy surface measure it is useful to transform the 'shifted' momenta $(p_x + y,\, p_y - x)$ to polar coordinates according to

$$p\cos\varphi = p_x + y, \qquad p\sin\varphi = p_y - x. \tag{6}$$

This gives

$$\begin{aligned}\delta(E - H)\,\mathrm{d}x\,\mathrm{d}y\,\mathrm{d}p_x\,\mathrm{d}p_y &= p\,\delta(E - H)\,\mathrm{d}x\,\mathrm{d}y\,\mathrm{d}p\,\mathrm{d}\varphi \\ &= \mathrm{d}x\,\mathrm{d}y\,\mathrm{d}\varphi \end{aligned} \tag{7}$$

with the understanding that the p integration has been carried out to remove the δ function and that the last measure is to be considered on the respective energy surface. Equation (7) means that the energy surface measure is constant in terms of (x, y, φ). The uniform distribution in the planetary neighbourhood can hence be obtained from an equidistribution in (x, y, φ). Because the boundary of the planetary energy surface component does not have a simple parametrization in terms of the variables (x, y, φ), we at first choose a box $[x_{\min}, x_{\max}] \times [y_{\min}, y_{\max}]$ which contains the complete projection of the planetary neighbourhood to configuration space. We then sample points (x, y, φ) randomly with an equidistribution in $[x_{\min}, x_{\max}] \times [y_{\min}, y_{\max}] \times [0, 2\pi]$ and check whether $[x, y, p_x = x + p\cos(\varphi), p_y = y - p\sin\varphi]$ with $p = [2(E - V)]^{1/2}$ is contained in the planetary neighbourhood. To check this we have to find out whether (x, y) lies between the zero velocity curves for the energy under consideration and, for points near L_1 and L_2, we have to find out whether they are on the correct side of the dividing surfaces. The latter check requires the transformation to NF coordinates.

For the energies $E = -4.4$, $E = -4.35$ and $E = -4.3$, Fig. 4 shows the resulting normalized histograms, or survival probabilities, $P_{\mathrm{s}}(t)$ of trajectories remaining in the planetary neighbourhood up to time t. The curves are monotonically decreasing and there is an ongoing debate whether the decay is exponential or algebraic (Heggie 2001). Rather than studying the functional form of the decay, we want to focus on the energy-dependent values $P_{\mathrm{s};\infty}$ at which the survival probabilities saturate for $t \to \infty$. For each energy the value $P_{\mathrm{s};\infty}$ can be interpreted as the fraction of the total energy surface volume of the planetary neighbourhood which consists of bound initial conditions, i.e. initial conditions which, when integrated in time, lead to trajectories which do not escape. Similarly, $1 - P_{\mathrm{s};\infty}$ is the fraction of initial conditions which do escape.

The main point of this paper is to present a procedure to compute the energy surface volume of escaping initial conditions which is simpler and computationally cheaper than the brute-force method above. This procedure utilizes the phase-space structures mentioned in Sections 2 and 3.1 and, as we will see in Sections 4.1 and 4.2, a generalization of this method also applies to the spatial system. To

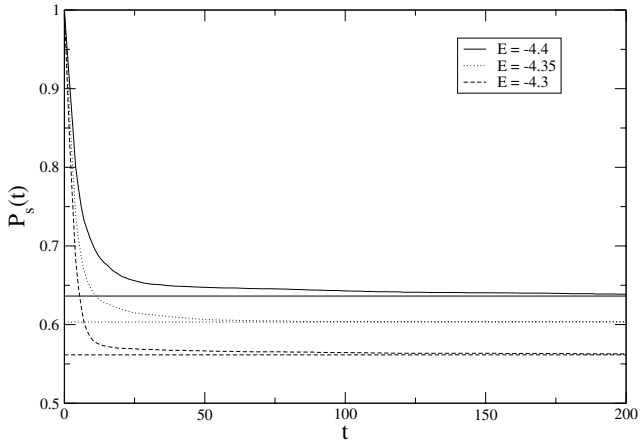

Figure 4. Planar Hill's problem. Survival probability curve $P_{\mathrm{s}}(t)$ for a uniform distribution of initial conditions in the planar planetary neighbourhood. The limiting values (horizontal lines) are computed from the procedure described in Section 3.2.

understand the procedure, it is important to note at first that, except for a set of measure zero, all escaping initial conditions not only lead to escape when integrated forward in time but also leave the planetary neighbourhood when integrated backward in time. This is essentially a consequence of Liouville's theorem on the conservation of phase-space volume (Arnold 1978) and means that almost all escaping trajectories coincide with capture trajectories, i.e. with trajectories which enter the planetary neighbourhood from the unbound region through either of the dividing surfaces $S^2_{\mathrm{ds}}(\mathrm{L}_1)$ or $S^2_{\mathrm{ds}}(\mathrm{L}_2)$ and become temporarily trapped in the planetary neighbourhood.

As mentioned in Section 3.1, the escaping trajectories and captured trajectories are enclosed by the escape and capture cylinders, respectively. These cylinders become extremely distorted if they are followed from the neighbourhood of the Lagrange points far into the planetary neighbourhood. In fact, the 'inward' branches of the stable and unstable manifolds, i.e. the branches $W^{\mathrm{s}}_{\mathrm{e}}(\mathrm{L}_1)$, $W^{\mathrm{s}}_{\mathrm{e}}(\mathrm{L}_2)$, $W^{\mathrm{u}}_{\mathrm{c}}(\mathrm{L}_1)$ and $W^{\mathrm{u}}_{\mathrm{c}}(\mathrm{L}_2)$ directed from the NHIMs into the planetary neighbourhood, intersect in a highly complex way forming a homoclinic and a heteroclinic tangle, the paradigms of chaos (Wiggins 1988, 1990a). Still, as will show in more detail, the stable and unstable manifolds separate escaping from non-escaping trajectories, and, for the escaping trajectories, determine for how long they become temporarily trapped in the planetary neighbourhood. In order to demonstrate this, we introduce an important concept, which is based on taking the dividing surfaces near L_1 and L_2 as surfaces of section. We call these surfaces of section 'dividing surfaces of section' (DSOS). In general, the choice of a surface of section involves a great deal of arbitrariness. However, for transport across a saddle the special choice of taking the dividing surface as the surface of section is singled out by its direct physical significance as the bottleneck to escape and capture. In fact, the usual restriction to one direction of traversal leads to either an escape or a capture hemisphere. These hemispheres are good surfaces of section in the sense of Birkhoff (1917, 1922) as they are everywhere transverse to the Hamiltonian flow except for their boundaries (the NHIM) which themselves are invariant under the flow. A DSOS can be considered as a surface of section which is 'dual' to the more familiar choice which is transverse to the NHIM. The latter is used to study the homoclinic and/or heteroclinic tangle and it is the starting point for studies of phase-space transport in terms of lobe dynamics (Wiggins

1992). However, we note that it is not always possible to define a surface of section 'sufficiently global' for which the lobe dynamics approach can be applied. The problem becomes even more severe in three dimensions.

More precisely, we study initial conditions on the capture hemisphere $B_c^2(L_1)$, i.e. initial conditions which lead to trajectories that leave the neighbourhood of L_1 and enter the planetary neighbourhood. We integrate the equations of motion for these initial conditions for the time it takes the resulting trajectory to reach either of the dividing surfaces near L_1 and L_2. The resulting time is thus the passage time, i.e. the time a trajectory spends in the planetary neighbourhood between entering the planetary neighbourhood through the dividing surface $S_{ds}^2(L_1)$ and escaping the planetary neighbourhood through either $S_{ds}^2(L_1)$ or $S_{ds}^2(L_2)$. Note that for the above mentioned reasons of phase-space volume conservation, the trajectories for all but a set of measure zero of initial conditions on $B_c^2(L_1)$ have to escape the planetary neighbourhood after spending some time in the planetary neighbourhood. This way we obtain a passage time map $B_c^2(L_1) \to \mathbb{R}$, $(q_2, p_2) \mapsto t(q_2, p_2)$ where we use the NF coordinates (q_2, p_2) to parametrize $B_c^2(L_1)$. Fig. 5 shows the contours of this map for the same energies as in Fig. 4. Initial conditions that lead to escape through the dividing surface near L_2 are marked blue with the time increasing from light blue to dark blue. Initial conditions that lead to escape through the dividing surface near L_1 are marked yellow/red with the time increasing from yellow to red.

The colour (and hence the passage times) changes smoothly within stripes and tongue shaped patches. The boundaries of the patches are double spirals. This means that if a boundary line is followed from a fixed starting point on the line, then the line starts to swirl, in a fashion reminiscent of a trajectory approaching a limit cycle, as it comes closer to the boundary of the DSOS $B_c^2(L_1)$. The passage time diverges at these double spirals. In fact, the double spirals are the intersections of the stable manifolds of the Lyapunov periodic orbits (the NHIMs) near L_1 and L_2 with $B_c^2(L_1)$. In order to show this, we compute these intersections by 'globalizing' $W_e^s(L_1)$ and $W_e^s(L_2)$ obtained from the NF in the neighbourhoods of L_1 and L_2 using Hill's equations as described in Section 2. The result of this computation is shown in Fig. 5(b). It shows a clear agreement with the structure of the DSOS in Fig. 5(a). The swirling of the double spirals can now be understood from the behaviour of homoclinic and heteroclinic orbits, i.e. those orbits contained in $W_e^s(L_1)$ and $W_e^s(L_2)$, respectively, that, backward in time, are asymptotic to the Lyapunov periodic orbit of L_1. These orbits approach the Lyapunov orbit in a spiralling manner with the rate of spiralling logarithmically diverging upon approach of the Lyapunov periodic orbit. The closer the points in the intersections of $W_e^s(L_1)$ and $W_e^s(L_2)$ with the DSOS are to the boundary of the DSOS, the stronger the corresponding orbits temporarily imitate the homoclinic and heteroclinic orbits.

In order to see more clearly the divergence of the passage time upon approach of the stable manifold branches in the DSOS, Fig. 6 shows the passage times along the line $p_2 = 0$ of the DSOS with energy $E = -4.4$ in Fig. 5. The picture shows rather flat plateaux interrupted by logarithmic singularities of the passage time. The singularities correspond to orbits which in time are forward asymptotic to either of the Lyapunov periodic orbits near L_1 and L_2, i.e. to orbits which are contained in the escape branches $W_e^s(L_2)$ (blue) or $W_e^s(L_1)$ (red). The plateaux, and similarly the patches in Fig. 5, correspond to different families of orbits which, besides the exit $S_{ds}^2(L_1)$ or $S_{ds}^2(L_2)$ through which they escape, are basically characterized by the number of loops their configuration space projection perform about the planet. Fig. 7 shows as representative examples the orbits marked by the arrows in Fig. 6. As can be seen from the magnifications in Fig. 6, the stable manifolds organize these families in a complex self-similar structure that is well known from classical scattering theory; see the focus issue 'Chaotic Scattering' in 1997, Chaos, 3(4). In fact, between each two logarithmic singularities of the passage times, there is an infinity of further singularities which organize infinitely many plateaux of decreasing size.

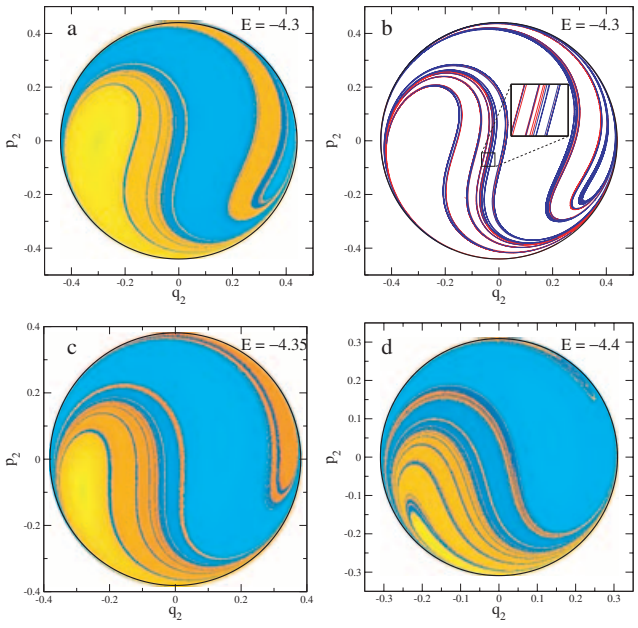

Figure 5. Planar Hill's problem. Passage time contours on the DSOS $B_c^2(L_1)$ for different energies E (a), (c) and (d). Yellow/red regions correspond to escape through the dividing surface near L_1 with the passage time increasing from yellow to red. Light blue/dark blue regions correspond to escape through the dividing surface near L_2 with the passage time increasing from light to dark blue. For $E = -4.3$ (b) shows the intersections of the stable manifolds of the Lyapunov periodic orbits near L_1 and L_2 with the DSOS.

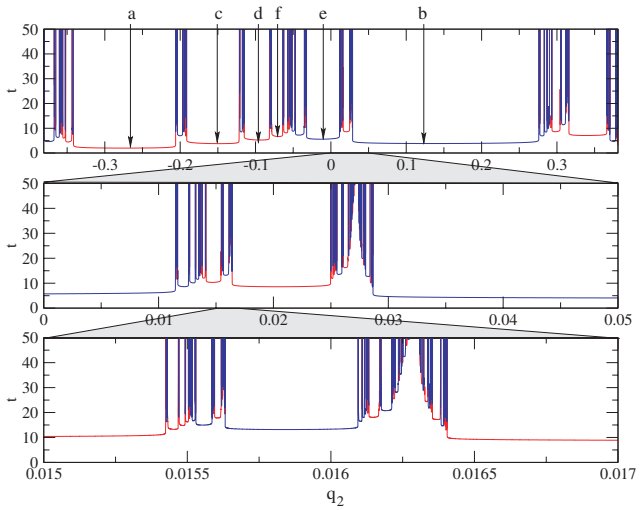

Figure 6. Planar Hill's problem. Passage times along the line $p_2 = 0$ in the DSOS with energy $E = -4.35$ in Fig. 5(c). As in Fig. 5, red segments of the graph correspond to exit through the dividing surface near L_1 and blue segments correspond to exit through the dividing surface near L_2. The middle and bottom panels show successive magnifications.

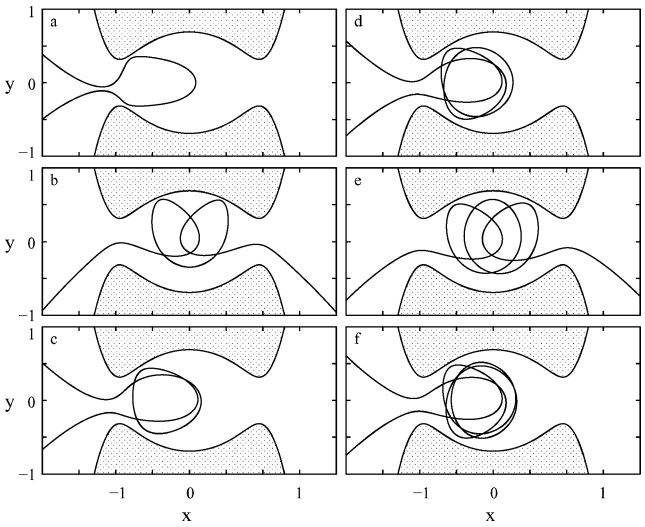

Figure 7. Planar Hill's problem. Configuration space projections of representative orbits as marked in the top panel of Fig. 6. The shaded regions are classically forbidden.

Each light blue/dark blue patch in $B_c^2(L_1)$ is mapped continuously to a patch in $B_e^2(L_2)$. Similarly, each yellow/red patch in $B_c^2(L_1)$ is mapped continuously to a patch in $B_e^2(L_1)$. We want to compute the energy surface volume swept out by letting the Hamiltonian flow act upon a patch in $B_c^2(L_1)$ until it reaches its image in $B_e^2(L_1)$ or $B_e^2(L_2)$, i.e. we want to compute the volume of the orbit segments with starting points in a patch in $B_c^2(L_1)$ and endpoints in $B_e^2(L_1)$ or $B_e^2(L_2)$. Pollak (1981) proves a result that shows that this volume is given by

$$\mathrm{vol}_{\mathrm{patch}} = \int_{\mathrm{patch}} t \, \mathrm{d}p_2 \, \mathrm{d}q_2, \tag{8}$$

i.e. the volume is given by the integral of the passage time $t(q_2, p_2)$ over the patch in $B_c^2(L_1)$. The divergence of the passage time at the boundary of the patches is too weak to spoil the existence of this integral. In fact, we can even sum over the infinite number of patches to obtain the volume vol_e of the set of initial conditions in the planetary neighbourhood occupied by initial conditions which lead to escape. More precisely, the sum of the volumes (8) over all patches in $B_c^2(L_1)$ gives at first the volume of all orbit segments in the planetary neighbourhoods which correspond to trajectories that entered the planetary neighbourhood through $B_c^2(L_1)$. Due to the symmetry (2), this volume is equal to the volume of all orbit segments in the planetary neighbourhoods which correspond to trajectories that entered the planetary neighbourhood through $B_c^2(L_2)$. We thus find the total volume of escaping initial conditions in the planetary neighbourhood to be

$$\mathrm{vol}_e = 2 \int_{B_c^2(L_1)} t \, \mathrm{d}p_2 \, \mathrm{d}q_2. \tag{9}$$

Defining the average passage time of initial conditions in $B_c^2(L_1)$ according to

$$\langle t \rangle_{B_c^2(L_1)} = \frac{\int_{B_c^2(L_1)} t \, \mathrm{d}p_2 \, \mathrm{d}q_2}{\int_{B_c^2(L_1)} \mathrm{d}p_2 \, \mathrm{d}q_2}, \tag{10}$$

with the denominator

$$\phi_{B_c^2(L_1)} = \int_{B_c^2(L_1)} \mathrm{d}p_2 \, \mathrm{d}q_2, \tag{11}$$

Table 1. Planar Hill's problem. For different energies E the table gives the results for the energy surface volume of the planetary neighbourhood vol_0, the mean passage time through the planetary neighbourhood $\langle t \rangle_{B_c^2(L_1)}$ for trajectories started on the dividing surface hemisphere $B_c^2(L_1)$, the flux $\phi_{B_c^2(L_1)}$ through $B_c^2(L_1)$, the volume of escaping initial conditions in the planetary neighbourhood vol_e computed according to equation (12), the fraction of bound initial conditions $1 - \mathrm{vol}_e/\mathrm{vol}_0$, and for initial conditions in $B_c^2(L_1)$, the probability $P_{1\to1}$ of the corresponding trajectory to escape the planetary neighbourhood through the dividing surface $S_{ds}^2(L_1)$ near L_1.

E	vol_0	$\langle t \rangle_{B_c^2(L_1)}$	$\phi_{B_c^2(L_1)}$	vol_e	$1 - \mathrm{vol}_e/\mathrm{vol}_0$	$P_{1\to1}$
−4.4	12.21	7.31	0.30	4.44	0.64	30 per cent
−4.35	13.05	5.67	0.46	5.18	0.60	41 per cent
−4.3	13.56	4.88	0.61	5.94	0.56	49 per cent

being the flux through $B_c^2(L_1)$ (see MacKay 1990; Waalkens & Wiggins 2004), we can rewrite equation (9) as

$$\mathrm{vol}_e = 2\phi_{B_c^2(L_1)} \langle t \rangle_{B_c^2(L_1)}. \tag{12}$$

The computation of the volume of escaping initial conditions in the planetary neighbourhood thus reduces to the computation of the flux $\phi_{B_c^2(L_1)}$ and the mean passage time $\langle t \rangle_{B_c^2(L_1)}$. This result, together with its generalization to the spatial Hill's problem in Section 4.2, is a key tool used in this paper.

The flux is easily computed from the NF. Applying the Stokes theorem yields the well-known result that the flux is given by the action of the Lyapunov periodic orbit, i.e.

$$\phi_{B_c^2(L_1)} = \int_{S^1_{\mathrm{NHIM}}(L_1)} \boldsymbol{p} \, \mathrm{d}\boldsymbol{q} = 2\pi J_2, \tag{13}$$

where we obtain J_2 from the NF as the solution of $E = H_{\mathrm{NF;planar}}(0, J_2)$. The results for $\phi_{B_c^2(L_1)}$ for the same energies as considered before in Fig. 4 are listed in Table 1.

The integral equation (10) can be computed by averaging the passage times over a sufficiently dense equidistant (p_2, q_2) grid in $B_c^2(L_1)$. Using the data that lead to the DSOS in Fig. 5, which consist of approximately 200 000 grid points for each energy, we obtain the results listed in Table 1. As expected, the mean passage $\langle t \rangle_{B_c^2(L_1)}$ decreases with energy while the flux $\phi_{B_c^2(L_1)}$ increases with energy.

With a procedure to compute vol_e we are now in a position to estimate the saturation values $P_{s;\infty}$ of the survival probabilities in Fig. 4. To this end it only remains to compute the energy surface volumes of the planetary neighbourhoods vol_0. However, these volumes are easily obtained as a byproduct of the procedure described above to compute the survival probability curves (see Section 4.2 which contains more details for the analogous computations for the spatial system). The results for vol_0 are also listed in Table 1.

According to our earlier reasoning, the saturation values $P_{s;\infty}$ of the survival probability curves should be equal to $1 - \mathrm{vol}_e/\mathrm{vol}_0$. In order to make this comparison, Fig. 4 shows (as the horizontal lines) the values $1 - \mathrm{vol}_e/\mathrm{vol}_0$ for the corresponding energies. In spite of our relatively naive procedure to compute the highly singular integral in equation (10), the agreement is excellent.

Moreover, using the data that lead to Fig. 5 we can compute the probability for a trajectory initialized in $B_c^2(L_1)$ to escape, after passing through the planetary neighbourhood, through dividing surface $S_{ds}^2(L_1)$ or $S_{ds}^2(L_2)$. Note that due to the symmetry (2) the initial conditions sampled uniformly in the planetary neighbourhood have equal probability to escape through the dividing surfaces $S_{ds}^2(L_1)$ or $S_{ds}^2(L_2)$. However, this does not imply an equiprobability for initial conditions in $B_c^2(L_1)$ to escape through $S_{ds}^2(L_1)$ or $S_{ds}^2(L_2)$. Table 1

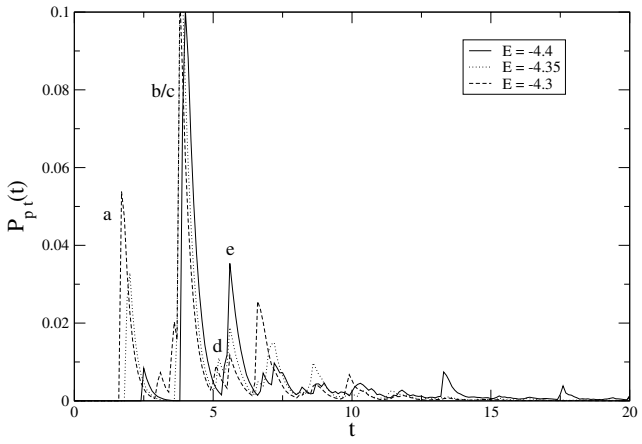

Figure 8. Planar Hill's problem. Passage time distribution $P_{\rm pt}(t)$ for initial conditions on the DSOS $B_{\rm c}^2(\mathrm{L}_1)$.

lists the results for the probabilities $P_{1\to1}$ for a trajectory started in $B_{\rm c}^2(\mathrm{L}_1)$ to escape through $S_{\rm ds}^2(\mathrm{L}_1)$. The probability $P_{1\to2}$ to escape through $S_{\rm ds}^2(\mathrm{L}_2)$ simply is $1 - P_{1\to1}$. $P_{1\to1}$ is related to the 'overlap' between the stable and unstable manifold branches $W_{\rm e}^{\rm s}(\mathrm{L}_1)$ and $W_{\rm c}^{\rm u}(\mathrm{L}_1)$. Table 1 shows a remarkable dependence of this overlap on energy with $P_{1\to1}$ decreasing as the energy decreases.

It is also interesting to compute the distributions $P_{\rm pt}(t)$ of passage times t for initial conditions on the DSOS $B_{\rm c}^2(\mathrm{L}_1)$. We show these distributions for the same three energies we used above in Fig. 8. The peaks of $P_{\rm pt}(t)$ can be identified with the biggest stripes and tongue-shaped patches in Fig. 5. To understand the peak structure it is important to note that the passage time varies only a little across a large part of a single patch, as can be seen from the flat plateaux of the passage times in Fig. 6. A single patch is therefore characterized essentially by a single passage time, which in turn corresponds to a single type of orbit like those shown in Fig. 7. For small times t, this enables us to assign the peaks by the orbits in Fig. 7. For large times, the distributions $P_{\rm pt}(t)$ consist of contributions from many different types of orbits so that an assignment of individual peaks in terms of representative orbits becomes impossible.

4 SPATIAL HILL'S PROBLEM

For the spatial Hill's problem, the motion in configuration space is confined by zero velocity surfaces, which are the level sets of the effective potential energy

$$V \equiv H - \frac{1}{2}|(p_x + y,\, p_y - x,\, p_z)|^2 = -\frac{3}{2}x^2 + \frac{1}{2}z^2 - \frac{3}{r} \qquad (14)$$

and which are shown in Fig. 9. For $E < E_0$ they bound a closed region about the origin. As in the planar case, this region opens for energies $E > E_0$. The bottlenecks to escape and capture are again given by the dividing surfaces near L_1 and L_2, which divide the energy surfaces for $E > E_0$ into three disjoint components. Again we use the middle component in our definition of the planetary neighbourhood for $E > E_0$.

4.1 Phase-space conduits for transport across the bottlenecks near L_1 and L_2 in the spatial system

For a fixed energy E slightly above E_0, Fig. 10 shows the generalizations of the manifolds near the saddle L_1 discussed in Section 3.1 for the planar system to the case of three DOF, now as projections

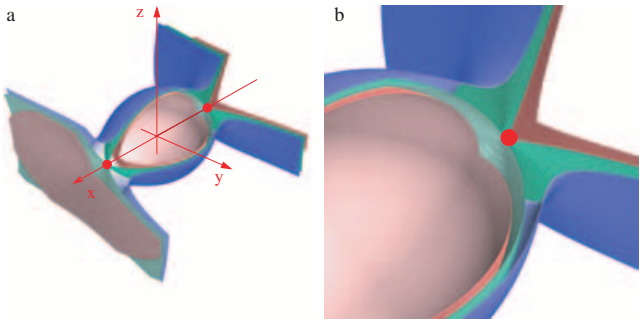

Figure 9. Spatial Hill's problem. Zero velocity surfaces of the spatial Hill's problem for energies $E = E_0 + n0.25$, $n = -1, 0, 1$ (a). The red balls mark L_1 and L_2. (b) shows a magnification of the region about L_1 in (a). For clarity, the region $y, z \geqslant 0$ is omitted in each image.

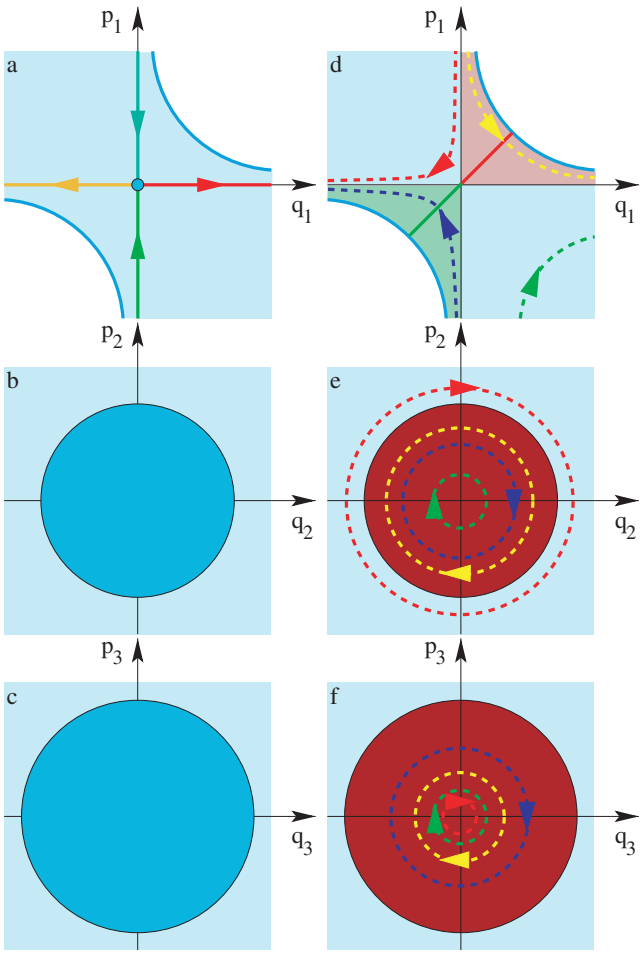

Figure 10. Spatial Hill's problem. Schematic plot of the manifolds near L_1 as projections to the NF coordinate planes. (a), (b) and (c) show the projections of the NHIM and its stable and unstable manifolds to the saddle and centre planes, respectively. (d), (e) and (f) show the projections of the dividing surface, the capture and escape cylinders and the volumes they enclose (see text). (d), (e) and (f) also show representative orbits: the dashed yellow line marks a captured orbit, the blue dashed line marks an escaping orbit, and the red and green dashed lines correspond to orbits that are not captured and do not escape, respectively. The colour scheme is the same as in Fig. 2.

to the saddle plane (q_1, p_1), and the centre planes (q_2, p_2) and (q_3, p_3). The colour scheme is the same as in Fig. 2. The projection of the energy surface is again marked light blue. In the saddle plane (q_1, p_1) the projection of the energy surface is bounded by the two branches of the hyperbola $p_1 q_1 = \mathcal{I}$ with $\mathcal{I}$ restricted to energy E implicitly defined by $H_{\rm NF}(\mathcal{I}, 0, 0) = E$; it is unbounded in the centre planes (q_2, p_2) and (q_3, p_3).

The dividing surface 4-sphere, which we denote by $S^4_{\rm ds}(\mathrm{L}_1)$, has $p_1 = q_1$. In the saddle plane, $S^4_{\rm ds}(\mathrm{L}_1)$ projects to the segment $q_1 = p_1$ with endpoints $q_1 = p_1 = \pm\sqrt{\mathcal{I}}$ with $\mathcal{I}$ restricted to energy E implicitly defined by $H_{\rm NF}(\mathcal{I}, 0, 0) = E$. The projection of $S^4_{\rm ds}(\mathrm{L}_1)$ to the centre planes are discs with boundaries $(p_2^2 + q_2^2)/2 = J_2$ with J_2 implicitly defined by $H_{\rm NF}\,(0, J_2, 0) = E$ in the centre plane (q_2, p_2) and with boundary $(p_3^2 + q_3^2)/2 = J_3$ with J_3 implicitly defined by $H_{\rm NF}\,(0, 0, J_3) = E$ in the centre plane (q_3, p_3).

The NHIM near L_1 is now a three-dimensional sphere and we denote it by $S^3_{\rm NHIM}(\mathrm{L}_1)$. It has $q_1 = p_1 = 0$ and hence projects to the origin in the saddle plane. In contrast to the planar case, the projection of the NHIM to the centre planes gives discs which coincide with the projections of the dividing surface $S^4_{\rm ds}(\mathrm{L}_1)$. The reason for this difference is that the spatial system has two centre DOF between which the energy can be arbitrarily distributed. For the NHIM in the planar system, all the energy has to be in the single centre DOF.

The NHIM $S^3_{\rm NHIM}(\mathrm{L}_1)$ divides $S^4_{\rm ds}(\mathrm{L}_1)$ into two hemispheres: a capture hemisphere $B^4_{\rm c}(\mathrm{L}_1)$ and an escape hemisphere $B^4_{\rm e}(\mathrm{L}_1)$. The hemispheres have the structure of four-dimensional open balls. In the saddle plane, they project to the parts $q_1 = p_1 > 0$ and $q_1 = p_1 < 0$, respectively, of the segment that corresponds to $S^4_{\rm ds}(\mathrm{L}_1)$. All trajectories which enter the planetary neighbourhood from the unbound region of negative x have to cross the capture hemisphere $B^4_{\rm c}(\mathrm{L}_1)$; all trajectories which escape from the planetary neighbourhood into the unbound region of negative x have to cross the escape hemisphere $B^4_{\rm e}(\mathrm{L}_1)$.

The NHIM has stable and unstable manifolds $W^{\rm s}(\mathrm{L}_1)$ and $W^{\rm u}(\mathrm{L}_1)$ with the structure of spherical cylinders $\mathbb{R} \times S^3$. They have $q_1 = 0$ and $p_1 = 0$, respectively. Their projections to the saddle plane coincide with the coordinate axes; their projections to the centre planes coincide with the projections of the NHIM and the dividing surface. As in the planar case, the stable and unstable manifolds each have two branches, which we again call capture and escape branches, respectively. Their identification in terms of the NF coordinates is the same as in the planar case. We use these branches to define capture spherical cylinder and escape spherical cylinder in the analogous way as in the planar case. These spherical cylinders now enclose the five-dimensional volumes of escaping and captured trajectories, respectively. These volumes project to the region enclosed by the branches of the hyperbola of the projection of the energy surface in the second and third quadrants of the saddle plane, respectively; their projections to the centre planes coincide with the projections of the dividing surface and the NHIM.

As mentioned in Section 2, for the linearized equations of motion near the Lagrange points the equations for (z, p_z) decouple from the planar system. The linear frequency associated with (z, p_z) is 2 and is thus slightly smaller than the linear frequency $\sqrt{2\sqrt{7} - 1} \approx 2.07$ associated with the Lagrange points in the planar system. As a result, for energies E slightly above E_0, the value J_2 defined by $H_{\rm NF}\,(0, J_2, 0) = E$ is slightly smaller than the value J_3 defined by $H_{\rm NF}\,(0, 0, J_3) = E$. The projections of the dividing surface $S^4_{\rm ds}(\mathrm{L}_1)$ and the NHIM $S^3_{\rm NHIM}(\mathrm{L}_1)$ to the centre plane (q_2, p_2) are hence slightly smaller than their projection to the centre plane (q_3, p_3).

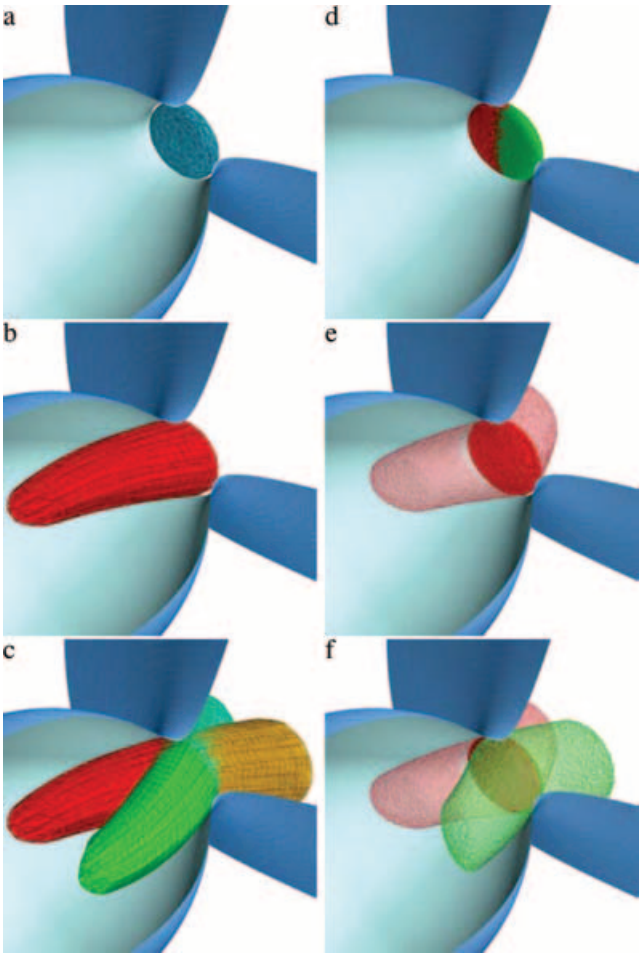

Figure 11. Spatial Hill's problem. High-dimensional cell-complexes (meshes) constructed on manifolds near L_1 projected to the (x, y, z) configuration space: (a) the NHIM $S^3_{\rm NHIM}(\mathrm{L}_1)$; (b) a piece of the unstable capture branch $W^{\rm u}_{\rm c}(\mathrm{L}_1)$; (c) pieces of the pairs of branches of the spherical cylinders $W^{\rm s}(\mathrm{L}_1)$ and $W^{\rm u}(\mathrm{L}_1)$; (d) the overlapping projections of the capture (red) and escape dividing surface hemisphere $B^4_{\rm c}(\mathrm{L}_1)$ and $B^4_{\rm e}(\mathrm{L}_1)$; (e) a piece of the projection of the energy surface volume enclosed by the capture spherical cylinder $W^{\rm s}_{\rm c}(\mathrm{L}_1) \cup W^{\rm u}_{\rm c}(\mathrm{L}_1)$; (f) pieces of the overlapping projections of the energy surface volumes enclosed by the capture spherical cylinder $W^{\rm s}_{\rm c}(\mathrm{L}_1) \cup W^{\rm u}_{\rm c}(\mathrm{L}_1)$ and the escape spherical cylinder $W^{\rm s}_{\rm e}(\mathrm{L}_1) \cup W^{\rm u}_{\rm e}(\mathrm{L}_1)$. The colour scheme is the same as in Fig. 10. The energy is $E = -4.4$.

Fig. 11 shows the manifolds computed from the NF as projections to the physical coordinates (x, y, z).

4.2 Escape from the planetary neighbourhood in the spatial system

We perform a study of escape for the spatial Hill's problem analogously to the planar case in Section 3.2. We start with a brute-force computation by sampling initial conditions uniformly in the planetary neighbourhood. The energy surface volume measure for the spatial system is $\delta(E - H)\,\mathrm{d}x\,\mathrm{d}y\,\mathrm{d}z\,\mathrm{d}p_x\,\mathrm{d}p_y\,\mathrm{d}p_z$. In order to achieve the uniform distribution with respect to this measure, we (successively) transform to spherical coordinates in the shifted momentum space

$$p\cos\varphi\sin\theta = p_x + y, \qquad p\sin\varphi\sin\theta = p_y - x,$$
$$p\cos\theta = p_z \tag{15}$$

as well as in coordinate space

$$r\cos\phi\sin\Theta = x, \qquad r\sin\phi\cos\Theta = y, \qquad r\cos\Theta = z. \quad (16)$$

Defining $\xi = -\cos\theta$ and $\zeta = -\cos\Theta$ this leads to

$$\delta(E - H)\ \mathrm{d}x\,\mathrm{d}y\,\mathrm{d}z\,\mathrm{d}p_x\,\mathrm{d}p_y\,\mathrm{d}p_z \quad (17)$$

$$= \sqrt{2(E - V)}\,\mathrm{d}x\,\mathrm{d}y\,\mathrm{d}z\,\mathrm{d}\xi\,\mathrm{d}\varphi \quad (18)$$

$$= \sqrt{2r^3\left[rE + \frac{3}{2}r^3\cos^2\phi(1-\zeta^2) - \frac{1}{2}r^3\zeta^2 + 3\right]}\ \times \mathrm{d}\phi\,\mathrm{d}\zeta\,\mathrm{d}r\,\mathrm{d}\xi\,\mathrm{d}\varphi \quad (19)$$

$$= \mathrm{d}R\,\mathrm{d}\phi\,\mathrm{d}\zeta\,\mathrm{d}\xi\,\mathrm{d}\varphi \quad (20)$$

again with the understanding that the p integration has been carried out to remove the δ function and that the remaining measures have to be considered on the respective energy surface. In the latter equation we substituted

$$R(r) = \int_0^r \mathrm{d}\tilde{r}\sqrt{2\tilde{r}^3\left[\tilde{r}E + \frac{3}{2}\tilde{r}^3\cos^2\Phi(1-\zeta^2) - \frac{1}{2}\tilde{r}^3\zeta^2 + 3\right]} \quad (21)$$

for r, and, having in mind Fubini's theorem with the R integration being carried out first, the function in equation (21) is considered to be a function of r only. Hence, the energy surface measure for the spatial system is constant in terms of $(R, \phi, \zeta, \xi, \varphi)$. Similar to the planar case, we sample points

$$(R, \phi, \zeta, \xi, \varphi) \in [0, R_{\max}] \times [0, 2\pi] \times [-1, 1] \times [-1, 1] \times [0, 2\pi] \quad (22)$$

where $R_{\max} = 1.3$ is a constant, which we have chosen sufficiently large so that the hypercube (22) includes the complete planetary neighbourhood for the energy under consideration. For each such point, we then check whether the corresponding point (x, y, z, p_x, p_y, p_z) on the energy surface $H = E$ is contained in the planetary neighbourhood. This check is slightly more involved than in the planar case because it requires us to invert equation (21) to compute r from $(R, \phi, \zeta, \xi, \varphi)$. Near L_1 and L_2, the check again requires the transformation to NF coordinates in order to see whether the point is on the correct side of the dividing surfaces $S^4_{\mathrm{ds}}(L_1)$ and $S^4_{\mathrm{ds}}(L_2)$, respectively. The points in the planetary neighbourhood are then integrated in time until they reach either one of the dividing surfaces near L_1 and L_2 or a large fixed cut-off time which we choose to be $t_{\mathrm{cut-off}} = 50\,000$.

Fig. 12 shows the resulting survival probability curves. As in the planar systems, the survival probabilities saturate for $t \to \infty$ at values $P_{\mathrm{s};\infty}$ which depend on the energy. A significant difference to the planar case is the much longer time the survival probabilities take to saturate in the spatial case. A possible explanation is that for the energies under considerations there still might exist an extended Arnol'd web of invariant tori in which the trajectories can become trapped for long times before they escape (see Simó & Stuchi 2000 for a study of the survival of tori in the planetary neighbourhood for energies above E_0 in the planar Hill's problem). As in the planar case we want to focus on the values $P_{\mathrm{s};\infty}$ and not on the functional form of the decay of the survival probabilities. As we will demonstrate, the values $P_{\mathrm{s};\infty}$ can be computed from a generalization of the procedure explained in Section 3.2. In fact, the classical spectral theorem of Pollak (1981) applies to systems with an arbitrary (finite) number of DOF. Accordingly, the volume of initial conditions in the planetary neighbourhood which lead to escaping trajectories can be computed from the 3-DOF version of equation (12), i.e.

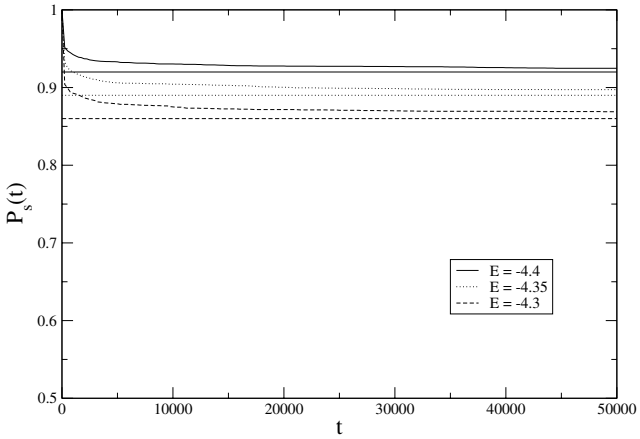

Figure 12. Spatial Hill's problem. Survival probability curve $P_{\mathrm{s}}(t)$ for a uniform distribution of initial conditions in the spatial planetary neighbourhood. The limiting values (horizontal lines) are computed from the procedure described in Section 4.2.

Table 2. Spatial Hill's problem. The analogous results of Table 1 now for the spatial Hill's problem.

E	vol_0	$\langle t\rangle_{B^4_{\mathrm{c}}(L_1)}$	$\phi_{B^4_{\mathrm{c}}(L_1)}$	$\mathrm{vol}_{\mathrm{e}}$	$1 - \mathrm{vol}_{\mathrm{e}}/\mathrm{vol}_0$	$P_{1\to1}$
−4.4	33.05	28.87	0.05	2.60	0.92	30 per cent
−4.35	34.34	17.90	0.11	3.86	0.89	33 per cent
−4.3	35.71	13.25	0.19	5.23	0.86	39 per cent

$$\mathrm{vol}_{\mathrm{e}} = 2\phi_{B^4_{\mathrm{c}}(L_1)}\langle t\rangle_{B^4_{\mathrm{c}}(L_1)}, \quad (23)$$

where $\phi_{B^4_{\mathrm{c}}(L_1)}$ is now the flux through the four-dimensional dividing surface hemisphere $B^4_{\mathrm{c}}(L_1)$ and $\langle t\rangle_{B^4_{\mathrm{c}}(L_1)}$ is the average passage time defined analogously to equation (10) but now as an integral over the four-dimensional hemisphere $B^4_{\mathrm{c}}(L_1)$.

The flux is easily obtained from the NF. According to Waalkens & Wiggins (2004) it is given by

$$\phi_{B^4_{\mathrm{c}}(L_1)} = (2\pi)^2\mathcal{A} \quad (24)$$

with $\mathcal{A}$ being the area in the space of the actions (J_2, J_3) enclosed by the contour $H_{\mathrm{NF}}(0, J_2, J_3) = 0$. We list the results in Table 2.

We compute $\langle t\rangle_{B^4_{\mathrm{c}}(L_1)}$ from a Monte Carlo computation. We therefore randomly start a large number n of trajectories in $B^4_{\mathrm{c}}(L_1)$ with a uniform distribution with respect to the measure $\mathrm{d}p_2\,\mathrm{d}p_3\,\mathrm{d}q_2\,\mathrm{d}q_3$. Note that $B^4_{\mathrm{c}}(L_1)$ can be parametrized by the NF coordinates (q_2, q_3, p_2, p_3) and that the measure $\mathrm{d}p_2\,\mathrm{d}p_3\,\mathrm{d}q_2\,\mathrm{d}q_3$ is the right measure for computing the flux (MacKay 1990; Waalkens & Wiggins 2004).

For these points we compute the passage times t_k, $k = 1, \ldots, n$, by integrating trajectories with these initial conditions until they reach either $B^4_{\mathrm{e}}(L_1)$ or $B^4_{\mathrm{e}}(L_2)$. We then take the arithmetic mean

$$\langle t\rangle_{B^4_{\mathrm{c}}(L_1);n} = \frac{1}{n}\sum_{k=1}^{n} t_k. \quad (25)$$

Fig. 13 illustrates the convergence of this procedure. Table 2 lists the 'limiting values' which we define to be $\langle t\rangle_{B^4_{\mathrm{c}}(L_1);1\,500\,000}$ as well as the resulting volumes of escaping initial conditions $\mathrm{vol}_{\mathrm{e}}$ computed according to equation (23).

In order to determine the saturation values $P_{\mathrm{s};\infty}$ of the survival probability curves, we also need the total energy surface volume of

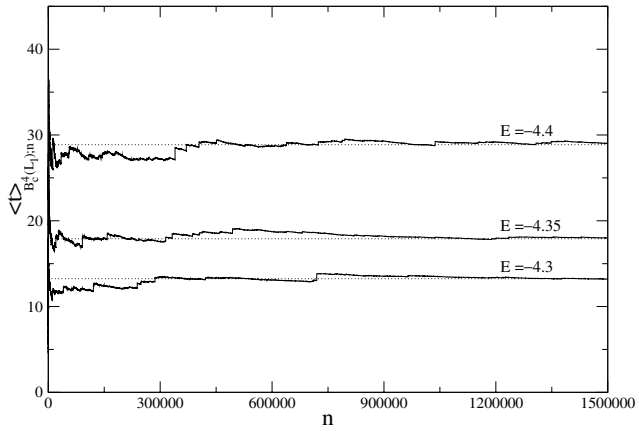

Figure 13. Spatial Hill's problem. Convergence of the mean passage time $\langle t \rangle_{B_c^4(L_1);n}$ for a Monte Carlo computation using equation (25). The dotted horizontal lines mark $\langle t \rangle_{B_c^4(L_1);1\,500\,000}$.

the planetary neighbourhood. As in the planar case, this volume can be obtained from the same sampling procedure we used to compute the survival probability curves. The difference is that we do not integrate the sampling points in time but only check whether they are contained in the planetary neighbourhood or not. The computational effort is therefore considerably smaller than in the computation of the survival probability curves. We thus consider the limiting value of

$$\mathrm{vol}_{0;n} = \frac{\#[(x_k, y_k, z_k, p_{x;k}, p_{y;k}, p_{z;k}) \in N : k \leqslant n]}{n}\,\mathrm{vol}_{\mathrm{hcube}} \qquad (26)$$

where N is the planetary neighbourhood and $\mathrm{vol}_{\mathrm{hcube}} = 16R_{\max}\pi^2$ is the volume of the hypercube (22). Fig. 14 illustrates the convergence of this procedure. Table 2 lists the 'limiting values' for which we take the values $\mathrm{vol}_{0;500\,000}$.

As in the planar case, we compare our results for the volume of escaping initial conditions $1 - \mathrm{vol}_e/\mathrm{vol}_0$ obtained by the above procedure with the saturation values of the survival probabilities $P_{s;\infty}$ by plotting them as horizontal lines in the survival probability graphs (see Fig. 12). The agreement is again very good.

It is worth mentioning that the escape branches $W_e^s(L_1)$ and $W_e^s(L_2)$ of the stable manifolds of the NHIMs at L_1 and L_2 partition the DSOS $B_c^4(L_1)$ [and analogously the DSOS $B_c^4(L_2)$] in the spatial

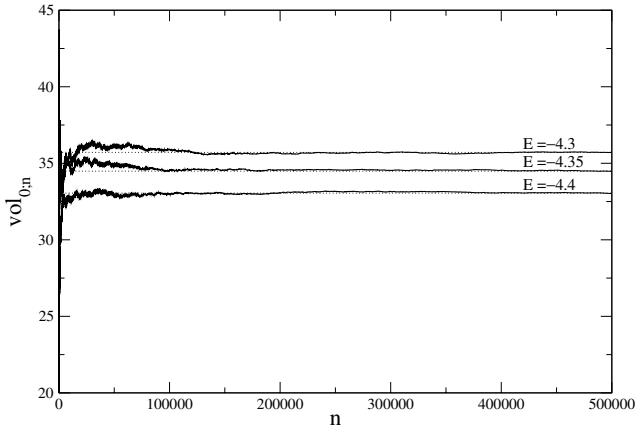

Figure 14. Spatial Hill's problem. Convergence of the planetary energy surface volume $\mathrm{vol}_{0;n}$ for a Monte Carlo computation using equation (26). The dotted horizontal lines mark $\mathrm{vol}_{0;500\,000}$.

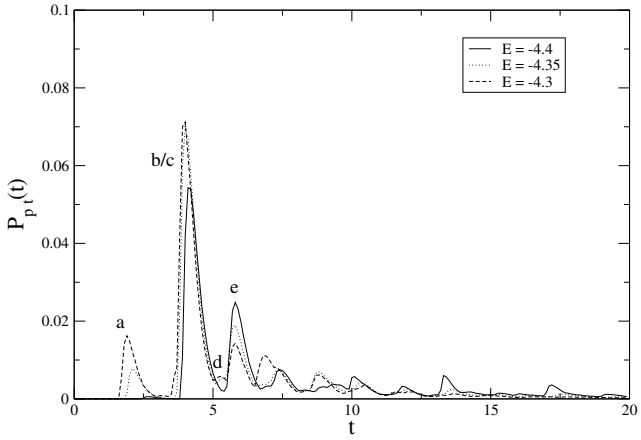

Figure 15. Spatial Hill's problem. Passage time distribution $P_{\mathrm{pt}}(t)$ for initial conditions on the DSOS $B_c^4(L_1)$.

Hill's problem in a similar way as in the planar system for which we illustrated the partitioning in Figs 5 and 6. In the spatial case, the intersections of $W_e^s(L_1)$ and $W_e^s(L_2)$ with the four-dimensional DSOS are three-dimensional. Due to the high dimensionality it is only possible to show sections through or projections of the four-dimensional DSOS. For example, the passage time along a one-dimensional line in $B_c^4(L_2)$ would give a picture similar to Figs 6. In fact, the line of initial conditions which leads to Figs 6 is also contained in the spatial DSOS (the spatial system contains the planar system as an invariant subsystem). Instead of providing a picture of another section for the spatial case, we present in Fig. 15 the passage time distribution $P_{\mathrm{pt}}(t)$ for initial conditions on the DSOS $B_c^4(L_1)$. It shows a similar peak structure as in the planar case with the peaks being broader, and hence of less height, than in the planar case, which is due to motion in the z-direction that is not present in the planar case.

5 CONCLUSIONS

In this paper we have shown how one can give a precise dynamical, and quantitative, description of escape and capture from a planetary neighbourhood using ideas from phase-space transport theory. In particular, dividing surfaces of (locally) no return have been constructed, which control transport into and out of the planetary neighbourhood. The construction method, via normalization, yields explicitly the parts of these surfaces responsible for capture and escape. Sampling only these parts of the dividing surfaces gives an efficient method to quantitatively study escape from a planetary neighbourhood. By making use of the classical spectral theorem of Pollak (1981), the methods we present allow one to compute, for example, the volume of unbound orbits in the planetary neighbourhood. The methods in this paper provide a highly computationally efficient alternative to procedures based on time-consuming brute-force Monte Carlo sampling of the entire planetary neighbourhood.

We have illustrated the methods by applying them to escape from the planetary neighbourhood in the two-dimensional and three-dimensional Hill's problem. The results of our computations, which we carried out for three different energies, are summarized in Tables 1 and 2.

As one might expect, in both the planar and the spatial Hill's problem, the proportion of initial conditions that lead to bound motion in the planetary neighbourhood decreases with energy (or equivalently,

the proportion of initial conditions that lead to unbound motion increases with energy). However, for each energy studied in this paper, the proportion of bound initial conditions in the spatial system is about 50 per cent larger than it is in the planar case. Similarly, the mean time that trajectories started on a dividing surface near one of the Lagrange points spend in the planetary neighbourhood (the mean passage time) decreases with energy. For the energies studied in this paper, the mean passage time for the spatial system is about three times larger than it is for the planar system. Moreover, we have studied the probability for a trajectory that is started on a dividing surface near one Lagrange point to escape the planetary neighbourhood, at a later point in time, through the same dividing surface, i.e. 'across' the same Lagrange point 'across' which it entered. In both the planar and spatial systems, this probability is well below 50 per cent and it increases with energy, where the increase is stronger in the planar case.

We remark that the results presented in this study are applicable to any problem with the same type of phase-space structure. This structure must be relevant to a particular transport question, which is generally a problem-dependent question. In particular, the results for the volume of escaping initial conditions also apply to scattering systems with several, not necessarily symmetry-related, entrance/exit channels. In this case equations (12) and (23) are replaced by a sum over the flux and mean passage times of the different entrance channels.

ACKNOWLEDGMENTS

This research was supported by ONR Grant No. N00014-01-1-0769. HW acknowledges support by the Deutsche Forschungsgemeinschaft Grant No. Wa 1590/1-1.

REFERENCES

Arnold V. I., 1978, Graduate Texts in Mathematics, Vol. 60, Mathematical Methods of Classical Mechanics. Springer-Verlag, Berlin
Arnol'd V. I., Kozlov V. V., Neishtadt A. I., 1988, in Arnol'd V. I., ed., Encyclopaedia of Mathematical Sciences, Vol. 3, Mathematical Aspects of Classical and Celestial Mechanics. Springer-Verlag, Berlin
Astakhov S. A., Farrelly D., 2004, MNRAS, 354, 971
Astakhov S. A., Burbanks A. D., Wiggins S., Farrelly D., 2003, Nat, 423, 264
Belbruno E., Marsden B. G., 1997, AJ, 113, 1433
Birkhoff G. D., 1917, Trans. Am. Math. Soc., 18, 199
Birkhoff G. D., 1922, Acta Math., 43, 1
Birkhoff G. D., 1927, Dynamical Systems. American Mathematical Society, Providence, RI
Child M. S., Pollak E., 1980, J. Chem. Phys., 73, 4365
Cordeiro R. R., Martins R. V., Leonel E. D., 1999, AJ, 117, 1634
Eyring H., 1934, J. Chem. Phys., 3, 107
Gustavson F., 1966, AJ, 71, 670
Heggie D. C., 2001, in Steves B., Maciejewski A., eds, Proc. 54th Scottish Univ. Summer School in Physics, The Restless Universe. IOP Publishing, Bristol, p. 109
Hénon M., 1969, A&A, 1, 223
Henrard J., Navarro J. F., 2001, Celest. Mech. Dyn. Astron., 79, 297
Heppenheimer T. A., Porco C., 1977, Icarus, 30, 385
Jaffé C., Farrelly D., Uzer T., 1999, Phys. Rev. A, 60, 3833
Jaffé C., Farrelly D., Uzer T., 2000, Phys. Rev. Lett., 84, 610
Jaffé C., Ross S. D., Lo M. W., Marsden J., Farrelly D., Uzer T., 2002, Phys. Rev. Lett., 89, 011101
MacKay R. S., 1990, Phys. Lett. A, 145, 425
Makó Z., Szenkovits F., 2004, Celest. Mech. Dyn. Astron., 90, 51
Murison M. A., 1989, AJ, 98, 2346
Murray C. D., Dermott S. F., 1999, Solar System Dynamics. Cambridge Univ. Press, Cambridge
Pechukas P., 1976, in Miller W. H., ed., Dynamics of Molecular Collisions. Plenum Press, New York
Pechukas P., McLafferty F. J., 1973, J. Chem. Phys., 58, 1622
Pechukas P., Pollak E., 1978, J. Chem. Phys., 69, 1218
Petit J.-M., Hénon M., 1986, Icarus, 66, 536
Pollak E., 1981, J. Chem. Phys., 74, 6763
Pollak E., Child M. S., Pechukas P., 1980, J. Chem. Phys., 72, 1669
Rüssmann H., 1964, Math. Ann., 154, 285
Siegel C. L., 1952, Nachr. Akad. Wiss. Göttingen, Math. Phys. Kl., 21
Siegel C. L., 1954, Math. Ann., 128, 144
Simó C., Stuchi T. J., 2000, Physica D, 140, 1
Stiefel E. L., Scheifele G., 1971, Linear and Regular Celestial Mechanics. Springer-Verlag, Berlin
Tanikawa K., Kikuchi N., Sato I., 1991, Icarus, 94, 112
Uzer T., Jaffé C., Palacián J., Yanguas P., Wiggins S., 2001, Nonlinearity, 15, 957
Waalkens H., Wiggins S., 2004, J. Phys. A, 37, L435
Waalkens H., Burbanks A., Wiggins S., 2004, J. Chem. Phys., 121, 6207
Wiggins S., 1988, Global Bifurcations and Chaos: Analytical Methods. Springer-Verlag, Berlin
Wiggins S., 1990a, Introduction to Applied Nonlinear Dynamical Systems and Chaos. Springer-Verlag, Berlin
Wiggins S., 1990b, Physica D, 44, 471
Wiggins S., 1992, Chaotic Transport in Dynamical Systems. Springer-Verlag, Berlin
Wiggins S., 1994, Normally Hyperolic Invariant Manifolds in Dynamical Systems. Springer-Verlag, Berlin
Wiggins S., Wiesenfeld L., Jaffé C., Uzer T., 2001, Phys. Rev. Lett., 86, 5478
Wigner E., 1937, J. Chem. Phys., 5, 720
Wigner E., 1938, Trans. Faraday Soc., 34, 29
Winter O. C., Neto E. V., 2001, A&A, 377, 1119
Yu Q., Tremaine S., 2001, AJ, 121, 1736

This paper has been typeset from a TEX/LATEX file prepared by the author.